Open Access

Iraqi Journal of Industrial Research (IJOIR)

Journal homepage: http://ijoir.gov.iq

# Study of the Linear Attenuation Coefficient for Gamma Rays, X-Rays, and Neutrons of Different Refractory Alloys via Computerized Phy-X, MATXCOM, and Ngcal Models

**Taher Toman Taher***

Iraqi Atomic Energy Commission, Iraq

**Article information**

***Article history:***
Received: February, 12, 2026
Accepted: May, 31, 2026
Available online: June, 14, 2026

***Keywords***:
W-Ni-Fe,
W-Ni-Cu,
Phy-X,
MATXCOM,
NGCal

***Corresponding Author:***
Taher Toman Taher
tahert4477@gmail.com

**DOI:**
**https://doi.org/10.53523/joirVol13I1ID645**



**Abstract**

In this study, the linear attenuation coefficient (LAC) of ten refractory alloys with different percentages of elements: 90W-7Ni-3Fe, 90W-6Ni-4Fe, 91W-6Ni-3Fe, 93W-4Ni-3Fe, 93W-5Ni-2Fe, 90W-6Ni-4Cu, 90W-5Ni-5Cu, 90W-7Ni-3Cu, 93W-4Ni-3Cu, and 95W-3Ni-2Cu were evaluated. These alloys contain a high tungsten with high density, and show minimal variations in tensile strength, elongation, and hardness. The LAC calculations were performed using Phy-X software for x-ray and radioisotopes with energy ranges of (0.00804 -15) MeV and (0.00589 -15) MeV, respectively, whereas MATXCOM software was used for the photon energy range (0.015-15) MeV. LAC for fast and thermal neutrons were explored via the NGCal platform with energy (4 MeV, 25.4 meV) respectively. The LAC was very high at low energies, then a subsequent gradual decrease as energy increased for all alloys. The difference of error (Δ %) depending on LAC data was calculated and compared between all tested software, where the (Δ %) results were within acceptable limits. Furthermore, the protection efficiency (PE %) was calculated at different thicknesses for all the tested alloys. According to LAC and PE% data, the 95W-3Ni-2Cu alloy appears as the best absorber of X-rays and Gamma rays, which contains the highest percentage of tungsten, density, and mean atomic number, whereas the 90W-7Ni-3Cu alloy shows the highest (PE %) of the fast and thermal neutrons. In conclusion, these alloys are suitable for mitigating the harmful effects of exposure to photons and neutrons, and for providing a safe working environment for radiation workers.

## 1. Introduction

The world today is witnessing tremendous technological advancements in various fields, which have contributed to the widespread dissemination of ionizing radiation. Exposure to this radiation poses a significant health risk, varying according to the dose, type of radiation, and duration of exposure. The dangers of radiation range from causing serious and immediate illnesses to increasing the risk of chronic health problems with exposure to enormous quantities. To ensure the highest level of safety for workers exposed to radiation, whether natural or industrial, it is essential to develop protective materials that can attenuate ionizing radiation and reduce its intensity [1, 2].

The use of these materials is crucial for achieving safe and acceptable levels of radiation for workers in nuclear reactors or laboratories. Exposure of the human body to neutrons is extremely dangerous due to their high ability to penetrate tissues, making them radioactive and thus causing damage to cells and genes. Protective materials significantly reduce the effects of neutrons or radiation, shorten their penetration distances through the material, and thus reduce the exposure risk. These materials should be compatible with the type and energy, readily available, easily manufactured, and inexpensive. Due to the shortcomings of traditional shielding materials, such as lead or concrete, in terms of durability and toxicity, many researchers have sought to develop new and alternative protective materials. This highlights the need to develop new types of protection materials, such as alloys that offer shielding, mechanical properties, and high heat resistance [3-6].

Acknowledging its unique physical properties, tungsten has emerged as a leading candidate for shielding. We have used various alloys containing tungsten in high contain. Its high density and large atomic number give it excellent absorption capacity for gamma rays and X-rays, thus effectively reducing their intensity. It has high heat resistance, allowing it to be used in high-temperature, radioactive environments, such as nuclear reactors. Tungsten has high mechanical strength, enabling the design of shields that can withstand harsh conditions without compromising performance. Thanks to these properties, a high level of protection can be achieved, eliminating the need for lead or concrete, while reducing the weight and size of the shields [7-9].

İ. Erkoyuncu [10] studied the interaction of gamma rays and neutrons with six alloys containing varying iron and nickel contents. These alloys are characterized by their durability and long lifespan. Shielding parameters, such as linear attenuation coefficient, mass attenuation coefficient, half-value layer, and tenth-value layer, were examined in an energy range of 0.06 to 2.614 MeV using WinXCOM, GEANT4, and FLUKA software. Neutron shielding parameters were also investigated using GEANT4 and FLUKA software in an energy range of 1.1 to 10 MeV. The Fe19Ni81 alloy was found to be the most effective against gamma rays and neutrons. The results showed that increasing the nickel content in iron-nickel alloys enhances gamma ray and neutron shielding, while reducing secondary radiation.

K. K. Hammud [11] Studied Six nickel alloys (Ni3Al, NiAl, Ni90Cr10, Ni80Cr20, Ni35Cr20Fe45, and Ni60Cr16Fe34) varied in their chemical formulas, mole fractions (%) of each element on using NGCal and Phy-X software for linear attenuation coefficient, mass attenuation coefficient, half-value layer, and tenth-value layer, were examined in an energy range of 1 to 15 MeV. The results indicated that Chromel (Ni90Cr10) alloy has the highest density, and a high Nickel mole fraction exhibited the highest protection efficiency.

Theoretically, we examined the attenuation effects of tungsten alloys via one of the most significant shielding coefficients, the linear attenuation coefficient, for ten distinct alloys featuring diverse alloying ratios across an energy spectrum spanning from 0.00804 MeV to 15 MeV for complex ternary tungsten refractory alloys. This was achieved using various computer platforms, such as Phy-X/PSD, MATXCOM, and NGCal. These programs are efficient in calculating radiation shielding factors (linear and mass attenuation coefficients, half-values, etc.) in addition to the protection from neutrons. They are user-friendly, cover a wide energy range for element and compound calculations, and are readily available online. This research paper enables radiation experts to select the most suitable alloys for radiation or neutron shielding whereas these alloys may be excellent suggestions to be used in radiation medicine, nuclear reactors, and aerospace applications besides radiation or neutron attenuation.

## 2. Experimental Procedure

Ten alloys containing tungsten as a primary element: (90W-7Ni-3Fe, 90W-6Ni-4Fe, 91W-6Ni-3Fe, 93W-4Ni-3Fe, 93W-5Ni-2Fe, 90W-6Ni-4Cu, 90W-5Ni-5Cu, 90W-7Ni-3Cu, 93W-4Ni-3Cu,and 95W-3Ni-2Cu) were tested, which were coded as W1,W2,W3,W4,W5,W6,W7,W8,W9, and W10, respectively.

Table (1) shows the most characteristic information related to the tested alloys, density, Tensile Strength Elongation, and Hardness, as well as the composition. Increasing the nickel and iron content in these tungsten alloys increases their density, improves their mechanical properties, and reduces cracking during manufacturing [12]. The mean atomic number $\mathbf{\bar{Z}}$ was computed according to references [13, 14].

Table (1) was adopted as the basis for comparing the alloys and provides an overview of the best materials for use in this field, including alloy properties such as chemical composition, density, and mean atomic number. From this, we can predict which materials are most effective in attenuating incident radiation and neutrons.

**Table (1):** Several characteristics of the tested alloys [13, 14].

| Code | Chemical formula | Density, gm/cm | Composition | | | Tensile Strength (MPa) | Elongation (%) | Hardness (HRC) | Mean Atomic Number, $\bar{Z}$ |
|---|---|---|---|---|---|---|---|---|---|
| | | | Weight Fraction of Elements | | Mole Fraction of Elements | | | | |
| W1 | 90W-7Ni-3Fe | 16.9 | W | 0.9000 | 0.7389 | 700 ~ 980 | 20 ~ 33 | 24 ~ 32 | 69.34 |
| | | | Ni | 0.0700 | 0.1800 | | | | |
| | | | Fe | 0.0300 | 0.0811 | | | | |
| W2 | 90W-6Ni-4Fe | 16.8 | W | 0.9000 | 0.7379 | 700 ~ 980 | 20 ~ 33 | 24 ~ 32 | 69.32 |
| | | | Ni | 0.0600 | 0.1541 | | | | |
| | | | Fe | 0.0400 | 0.1080 | | | | |
| W3 | 91W-6Ni-3Fe | 17.1 | W | 0.9100 | 0.7604 | 700 ~ 980 | 16 ~ 25 | 25 ~ 32 | 69.82 |
| | | | Ni | 0.0600 | 0.1570 | | | | |
| | | | Fe | 0.0300 | 0.0825 | | | | |
| W4 | 93W-4Ni-3Fe | 17.5 | W | 0.9300 | 0.8059 | 700 ~ 980 | 15 ~ 25 | 26 ~ 30 | 70.72 |
| | | | Ni | 0.0400 | 0.1086 | | | | |
| | | | Fe | 0.0300 | 0.0856 | | | | |
| W5 | 93W-5Ni-2Fe | 17.5 | W | 0.9300 | 0.8070 | 700 ~ 980 | 15 ~ 25 | 26 ~ 30 | 70.74 |
| | | | Ni | 0.0500 | 0.1359 | | | | |
| | | | Fe | 0.0200 | 0.0571 | | | | |
| W6 | 90W-6Ni-4Cu | 16.9 | W | 0.9000 | 0.7477 | 550 ~ 750 | 8 ~ 15 | 18 ~ 25 | 69.44 |
| | | | Ni | 0.0600 | 0.1561 | | | | |
| | | | Cu | 0.0400 | 0.0961 | | | | |
| W7 | 90W-5Ni-5Cu | 17 | W | 0.900 | 0.7492 | 550 ~ 750 | 8 ~ 16 | 18 ~ 23 | 69.45 |
| | | | Ni | 0.0500 | 0.1304 | | | | |
| | | | Cu | 0.0500 | 0.1204 | | | | |
| W8 | 90W-7Ni-3Cu | 17 | W | 0.900 | 0.7462 | 550 ~ 800 | 8 ~ 12 | 20 ~ 26 | 69.43 |
| | | | Ni | 0.0700 | 0.1818 | | | | |
| | | | Cu | 0.0300 | 0.0720 | | | | |
| W9 | 93W-4Ni-3Cu | 17.5 | W | 0.9300 | 0.8143 | 550 ~ 700 | 5 ~ 10 | 18 ~ 24 | 70.81 |
| | | | Ni | 0.0400 | 0.1097 | | | | |
| | | | Cu | 0.0300 | 0.0760 | | | | |
| W10 | 95W-3Ni-2Cu | 17.8 | W | 0.9500 | 0.8622 | 500 ~ 700 | 4 ~ 7 | 25 ~ 30 | 71.72 |
| | | | Ni | 0.0300 | 0.0853 | | | | |
| | | | Cu | 0.0200 | 0.0525 | | | | |

## 3. Theoretical Part

Theoretical studies take precedence over the practical side, as they represent the scientific basis for the specifications and properties of materials. They provide a general overview of different energy ranges, saving time and effort in selecting the best material before implementing the practical aspect.

The linear attenuation coefficient (LAC) indicates the degree to which radiation or neutron penetrates a material. Its high value indicates low penetration of the tested material, making it an ideal choice for manufacturing shields. In this research, the linear attenuation coefficient was calculated using three software: Phy-X, MATXCOM, and NGCal depend on the chemical composition of the compound, density, elemental ratios, attenuation coefficients, and energy range. Tables (2-5) present the LAC results for ten tested alloys at various energies obtained through the online Phy-X, MATXCOM, and NGCal programs. The difference of error (Δ %) depending on LAC data was calculated and compared between all computerized models, where the (Δ %) results were within satisfactory limits. Tables (6-9) and Figures (3-6) show the difference in error (Δ%).

Phy-X/PSD is a free and easy to use platform for calculating various photon radiation protection coefficients, including linear and mass absorption coefficients, the effective atomic number, and other dose parameters. It is based on reliable and global databases. With this fast, accurate, practical, and free software, any element, compound, or mixture can be analyzed via mole fraction or weight fraction. Furthermore, calculations can be done for different materials at the same time [15].

NGCal is a Natural Gamma Calculator, a free online software that is very useful for evaluating the shielding properties of materials against neutrons (thermal and fast) and photons (X-rays and gamma rays) at specific energies. It helps researchers and manufacturers to calculate attenuation coefficients (mass and line), mean free

path, and half- and tenth-value layers to design and develop safe and effective radiation shields. Incoherent scattering and absorption are considered in calculations for thermal and fast neutrons. Compton scattering, photoelectric absorption, and pair production are considered for photons. The Composition of materials can be defined by weight fraction and by empirical/molecular formulas. The simulation results of NGCal were found to be very similar to those of existing counterparts [16].

MATXCOM is a specialized computing tool for calculating gamma-rays and X-rays interaction parameters, such as linear attenuation coefficient (LAC), mass attenuation coefficient (MAC), half-value and tenth-value layers (HVL and TVL), mean free path (MFP), energy absorption and exposure accumulation coefficients (EABF and EBF), and atomic and electronic properties of various materials. It utilizes the EPICS2023 depending on the evaluated Photon Data Library (EPDL). MATXCOM features a simple and user-friendly input/output interface. It is implemented as a standalone program written in FORTRAN to achieve precise calculations for specific materials [17].

**Table (2):** LAC results of the X- rays shielding via each alloy according to Phy-X calculations.

| Energy Mev | | W1 | W2 | W3 | W4 | W5 | W6 | W7 | W8 | W9 | W10 |
|---|---|---|---|---|---|---|---|---|---|---|---|
| 8.04E-03 | $^{29}$Cu | 2771.650 | 2797.745 | 2824.888 | 2940.702 | 2888.531 | 2645.424 | 2661.585 | 2660.569 | 2801.568 | 2891.611 |
| 8.91E-03 | $^{29}$Cu | 2420.777 | 2398.500 | 2423.880 | 2428.294 | 2436.580 | 2282.537 | 2255.243 | 2336.843 | 2327.147 | 2356.581 |
| 1.34E-02 | $^{37}$Rb | 2973.405 | 2952.667 | 3023.725 | 3125.425 | 3128.701 | 2985.958 | 3004.397 | 3002.856 | 3137.631 | 3222.113 |
| 1.50E-02 | $^{37}$Rb | 2236.388 | 2220.837 | 2274.548 | 2351.688 | 2354.103 | 2245.588 | 2259.430 | 2258.321 | 2360.644 | 2424.877 |
| 1.50E-02 | | 2225.140 | 2209.668 | 2263.114 | 2400.787 | 2342.280 | 2234.291 | 2248.063 | 2246.961 | 2348.786 | 2412.708 |
| 1.74E-02 | $^{42}$Mo | 1501.204 | 1490.762 | 1526.985 | 1620.986 | 1580.732 | 1507.399 | 1516.694 | 1515.944 | 1585.138 | 1628.606 |
| 1.96E-02 | $^{42}$Mo | 1103.030 | 1095.354 | 1122.082 | 1191.907 | 1161.803 | 1107.629 | 1114.467 | 1113.899 | 1165.075 | 1197.237 |
| 2.00E-02 | | 1050.714 | 1043.402 | 1068.880 | 1135.519 | 1106.756 | 1055.099 | 1061.614 | 1061.071 | 1109.876 | 1140.550 |
| 2.21E-02 | $^{47}$Ag | 807.405 | 801.786 | 821.428 | 873.076 | 850.665 | 810.790 | 815.800 | 815.374 | 853.075 | 876.778 |
| 2.49E-02 | $^{47}$Ag | 589.910 | 585.810 | 600.222 | 638.403 | 621.715 | 592.373 | 596.036 | 595.721 | 623.470 | 640.928 |
| 3.00E-02 | | 362.087 | 359.581 | 368.490 | 392.408 | 381.824 | 363.571 | 365.819 | 365.625 | 382.881 | 393.753 |
| 3.21E-02 | $^{56}$Ba | 303.665 | 301.566 | 309.054 | 329.235 | 320.272 | 304.901 | 306.787 | 306.624 | 321.153 | 330.310 |
| 3.64E-02 | $^{56}$Ba | 217.360 | 215.862 | 221.244 | 235.861 | 229.323 | 218.231 | 219.580 | 219.465 | 229.944 | 236.555 |
| 4.00E-02 | | 169.554 | 168.388 | 172.599 | 184.100 | 178.930 | 170.223 | 171.275 | 171.186 | 179.407 | 184.597 |
| 4.45E-02 | $^{65}$Tb | 128.188 | 127.309 | 130.501 | 139.267 | 135.308 | 128.685 | 129.479 | 129.413 | 135.662 | 139.609 |
| 5.00E-02 | | 94.421 | 93.775 | 96.132 | 102.642 | 99.688 | 94.776 | 95.361 | 95.314 | 99.942 | 102.868 |
| 5.04E-02 | $^{65}$Tb | 92.570 | 91.937 | 94.248 | 100.633 | 97.735 | 92.918 | 93.491 | 93.445 | 97.983 | 100.853 |
| 6.00E-02 | | 58.868 | 58.468 | 59.941 | 64.034 | 62.167 | 59.078 | 59.441 | 59.414 | 62.317 | 64.154 |
| 8.00E-02 | | 119.939 | 119.207 | 122.569 | 133.785 | 127.937 | 120.030 | 120.746 | 120.735 | 128.002 | 132.710 |
| 1.00E-01 | | 68.199 | 67.784 | 69.689 | 76.028 | 72.730 | 68.246 | 68.652 | 68.647 | 72.762 | 75.429 |
| 1.50E-01 | | 24.411 | 24.263 | 24.933 | 27.120 | 25.996 | 24.424 | 24.569 | 24.568 | 26.005 | 26.935 |
| 2.00E-01 | | 12.193 | 12.119 | 12.444 | 13.474 | 12.957 | 12.198 | 12.269 | 12.270 | 12.960 | 13.405 |
| 3.00E-01 | | 5.117 | 5.086 | 5.214 | 5.582 | 5.410 | 5.118 | 5.148 | 5.149 | 5.410 | 5.577 |
| 4.00E-01 | | 3.091 | 3.072 | 3.143 | 3.330 | 3.251 | 3.090 | 3.108 | 3.109 | 3.250 | 3.340 |
| 5.00E-01 | | 2.242 | 2.228 | 2.277 | 2.391 | 2.348 | 2.241 | 2.253 | 2.255 | 2.348 | 2.407 |
| 6.00E-01 | | 1.795 | 1.784 | 1.822 | 1.900 | 1.875 | 1.795 | 1.805 | 1.806 | 1.874 | 1.918 |
| 8.00E-01 | | 1.342 | 1.334 | 1.360 | 1.407 | 1.397 | 1.341 | 1.349 | 1.350 | 1.396 | 1.424 |
| 1.00E+00 | | 1.110 | 1.103 | 1.124 | 1.156 | 1.152 | 1.109 | 1.115 | 1.116 | 1.151 | 1.173 |
| 1.50E+00 | | 0.845 | 0.839 | 0.855 | 0.875 | 0.875 | 0.844 | 0.848 | 0.849 | 0.874 | 0.889 |
| 2.00E+00 | | 0.748 | 0.743 | 0.757 | 0.775 | 0.775 | 0.747 | 0.751 | 0.752 | 0.774 | 0.788 |

| | | | | | | | | | | | |
|---|---|---|---|---|---|---|---|---|---|---|---|
| 3.00E+00 | | 0.682 | 0.678 | 0.691 | 0.712 | 0.709 | 0.683 | 0.685 | 0.686 | 0.708 | 0.722 |
| 4.00E+00 | | 0.672 | 0.667 | 0.681 | 0.704 | 0.699 | 0.671 | 0.675 | 0.676 | 0.699 | 0.713 |
| 5.00E+00 | | 0.679 | 0.675 | 0.688 | 0.715 | 0.708 | 0.679 | 0.683 | 0.683 | 0.708 | 0.723 |
| 6.00E+00 | | 0.694 | 0.690 | 0.704 | 0.733 | 0.724 | 0.694 | 0.698 | 0.698 | 0.724 | 0.740 |
| 8.00E+00 | | 0.733 | 0.728 | 0.744 | 0.777 | 0.766 | 0.733 | 0.737 | 0.738 | 0.766 | 0.784 |
| 1.00E+01 | | 0.775 | 0.770 | 0.787 | 0.824 | 0.811 | 0.775 | 0.780 | 0.780 | 0.811 | 0.831 |
| 1.50E+01 | | 0.874 | 0.868 | 0.888 | 0.934 | 0.916 | 0.875 | 0.880 | 0.880 | 0.917 | 0.940 |

**Table (3):** LAC results of the exposure to the photons released from various radioisotopes according to Phy-X calculations.

| Energy Mev | | W1 | W2 | W3 | W4 | W5 | W6 | W7 | W8 | W9 | W10 |
|---|---|---|---|---|---|---|---|---|---|---|---|
| 5.89E-03 | $^{(55)}$Fe | 5780.837 | 5742.365 | 5892.588 | 6119.132 | 6123.575 | 5798.417 | 5833.911 | 5831.544 | 6136.118 | 6330.295 |
| 5.90E-03 | $^{(55)}$Fe | 5753.987 | 5715.696 | 5865.229 | 6090.739 | 6095.161 | 5771.481 | 5806.809 | 5804.453 | 6107.641 | 6300.936 |
| 6.49E-03 | $^{(55)}$Fe | 4523.096 | 4493.065 | 4610.900 | 4788.914 | 4792.317 | 4536.575 | 4564.329 | 4562.509 | 4801.935 | 4954.660 |
| 6.54E-03 | $^{(55)}$Fe | 4443.178 | 4413.682 | 4529.456 | 4704.377 | 4707.715 | 4456.398 | 4483.660 | 4481.875 | 4717.148 | 4867.231 |
| 1.38E-02 | $^{(241)}$Am | 2740.341 | 2721.246 | 2786.824 | 2880.775 | 2883.775 | 2751.821 | 2768.805 | 2767.403 | 2891.941 | 2970.039 |
| 1.50E-02 | | 2225.140 | 2209.668 | 2263.114 | 2339.878 | 2342.280 | 2234.291 | 2248.063 | 2246.961 | 2348.786 | 2412.708 |
| 2.00E-02 | | 1050.714 | 1043.402 | 1068.880 | 1105.615 | 1106.756 | 1055.099 | 1061.614 | 1061.071 | 1109.876 | 1140.550 |
| 2.21E-02 | $^{(47)}$Ag | 807.405 | 801.786 | 821.428 | 849.789 | 850.665 | 810.790 | 815.800 | 815.374 | 853.075 | 876.778 |
| 2.31E-02 | $^{(109)}$Cd | 718.579 | 713.580 | 731.088 | 756.388 | 757.165 | 721.590 | 726.050 | 725.669 | 759.310 | 780.466 |
| 2.50E-02 | $^{(109)}$Cd | 583.732 | 579.675 | 593.939 | 614.584 | 615.211 | 586.169 | 589.793 | 589.482 | 616.947 | 634.228 |
| 2.55E-02 | $^{(109)}$ Cd | 554.155 | 550.305 | 563.856 | 583.478 | 584.073 | 556.466 | 559.906 | 559.610 | 585.718 | 602.147 |
| 2.63E-02 | $^{(241)}$Am | 508.979 | 505.446 | 517.907 | 535.965 | 536.509 | 511.096 | 514.256 | 513.984 | 538.017 | 553.143 |
| 3.00E-02 | | 362.087 | 359.581 | 368.490 | 381.445 | 381.824 | 363.571 | 365.819 | 365.625 | 382.881 | 393.753 |
| 3.08E-02 | $^{(133)}$Ba | 337.102 | 334.769 | 343.071 | 355.149 | 355.501 | 338.480 | 340.573 | 340.392 | 356.483 | 366.622 |
| 3.22E-02 | $^{(241)}$Am | 300.678 | 298.599 | 306.015 | 316.812 | 317.124 | 301.902 | 303.768 | 303.608 | 317.997 | 327.066 |
| 3.32E-02 | $^{(241)}$Am | 276.864 | 274.951 | 281.786 | 291.746 | 292.032 | 277.987 | 279.706 | 279.558 | 292.832 | 301.201 |
| 3.50E-02 | $^{(133)}$Ba | 240.846 | 239.184 | 245.140 | 253.828 | 254.075 | 241.816 | 243.311 | 243.183 | 254.767 | 262.073 |
| 3.54E-02 | $^{(133)}$Ba | 233.738 | 232.126 | 237.908 | 246.345 | 246.585 | 234.678 | 236.129 | 236.005 | 247.255 | 254.350 |
| 3.58E-02 | $^{(133)}$Ba | 226.920 | 225.355 | 230.970 | 239.167 | 239.399 | 227.831 | 229.240 | 229.119 | 240.049 | 246.942 |
| 3.95E-02 | $^{(152)}$Eu | 175.237 | 174.031 | 178.381 | 184.744 | 184.920 | 175.930 | 177.017 | 176.925 | 185.415 | 190.774 |
| 4.00E-02 | | 169.554 | 168.388 | 172.599 | 178.760 | 178.930 | 170.223 | 171.275 | 171.186 | 179.407 | 184.597 |
| 4.01E-02 | $^{(152)}$Eu | 168.217 | 167.060 | 171.238 | 177.352 | 177.520 | 168.881 | 169.924 | 169.836 | 177.993 | 183.143 |
| 4.59E-02 | $^{(152)}$Eu | 118.048 | 117.239 | 120.180 | 124.497 | 124.612 | 118.502 | 119.233 | 119.173 | 124.936 | 128.578 |
| 4.70E-02 | $^{(152)}$Eu | 110.707 | 109.949 | 112.709 | 116.762 | 116.870 | 111.131 | 111.816 | 111.760 | 117.171 | 120.591 |
| 4.96E-02 | $^{(133)}$Ba | 96.313 | 95.655 | 98.059 | 101.592 | 101.685 | 96.677 | 97.273 | 97.225 | 101.944 | 104.928 |
| 5.00E-02 | | 94.421 | 93.775 | 96.132 | 99.598 | 99.688 | 94.776 | 95.361 | 95.314 | 99.942 | 102.868 |
| 5.32E-02 | $^{(133)}$Ba | 80.473 | 79.924 | 81.935 | 84.894 | 84.970 | 80.771 | 81.269 | 81.229 | 85.183 | 87.683 |
| 5.95E-02 | $^{(241)}$Am | 60.042 | 59.634 | 61.136 | 63.351 | 63.406 | 60.257 | 60.627 | 60.599 | 63.560 | 65.433 |
| 6.00E-02 | | 58.868 | 58.468 | 59.941 | 62.113 | 62.167 | 59.078 | 59.441 | 59.414 | 62.317 | 64.154 |
| 8.00E-02 | | 119.939 | 119.207 | 122.569 | 127.914 | 127.937 | 120.030 | 120.746 | 120.735 | 128.002 | 132.710 |
| 8.10E-02 | $^{(133)}$Ba | 116.188 | 115.479 | 118.735 | 123.912 | 123.935 | 116.276 | 116.969 | 116.958 | 123.997 | 128.558 |
| 8.80E-02 | $^{(109)}$Cd | 94.040 | 93.466 | 96.099 | 100.285 | 100.303 | 94.108 | 94.669 | 94.661 | 100.351 | 104.038 |
| 9.90E-02 | $^{(241)}$Am | 70.008 | 69.581 | 71.537 | 74.646 | 74.659 | 70.056 | 70.473 | 70.468 | 74.693 | 77.431 |
| 1.00E-01 | | 68.199 | 67.784 | 69.689 | 72.717 | 72.730 | 68.246 | 68.652 | 68.647 | 72.762 | 75.429 |
| 1.03E-01 | $^{(241)}$Am | 63.281 | 62.895 | 64.662 | 67.469 | 67.480 | 63.323 | 63.700 | 63.695 | 67.510 | 69.982 |
| 1.22E-01 | $^{(152)}$Eu | 41.302 | 41.050 | 42.197 | 44.016 | 44.024 | 41.327 | 41.572 | 41.570 | 44.042 | 45.642 |
| 1.50E-01 | | 24.411 | 24.263 | 24.933 | 25.992 | 25.996 | 24.424 | 24.569 | 24.568 | 26.005 | 26.935 |
| 1.61E-01 | $^{(133)}$Ba | 20.616 | 20.491 | 21.054 | 21.942 | 21.946 | 20.626 | 20.748 | 20.748 | 21.953 | 22.732 |
| 2.00E-01 | | 12.193 | 12.119 | 12.444 | 12.955 | 12.957 | 12.198 | 12.269 | 12.270 | 12.960 | 13.405 |
| 2.23E-01 | $^{(133)}$Ba | 9.475 | 9.417 | 9.666 | 10.055 | 10.056 | 9.477 | 9.533 | 9.534 | 10.058 | 10.396 |
| 2.45E-01 | $^{(152)}$Eu | 7.759 | 7.712 | 7.913 | 8.225 | 8.226 | 7.761 | 7.807 | 7.808 | 8.228 | 8.498 |
| 2.76E-01 | $^{(133)}$Ba | 6.017 | 5.980 | 6.133 | 6.367 | 6.368 | 6.018 | 6.053 | 6.054 | 6.369 | 6.571 |
| 2.84E-01 | $^{(137)}$Cs | 5.718 | 5.683 | 5.827 | 6.049 | 6.050 | 5.719 | 5.752 | 5.753 | 6.050 | 6.241 |
| 2.84E-01 | $^{(131)}$I | 5.698 | 5.663 | 5.807 | 6.027 | 6.028 | 5.699 | 5.732 | 5.733 | 6.029 | 6.219 |
| 2.96E-01 | $^{(152)}$Eu | 5.256 | 5.224 | 5.355 | 5.556 | 5.557 | 5.256 | 5.287 | 5.288 | 5.557 | 5.730 |
| 3.00E-01 | | 5.117 | 5.086 | 5.214 | 5.409 | 5.410 | 5.118 | 5.148 | 5.149 | 5.410 | 5.577 |
| 3.03E-01 | $^{(133)}$Ba | 5.024 | 4.993 | 5.118 | 5.309 | 5.310 | 5.024 | 5.053 | 5.054 | 5.310 | 5.474 |
| 3.44E-01 | $^{(152)}$Eu | 3.969 | 3.944 | 4.040 | 4.185 | 4.185 | 3.969 | 3.991 | 3.993 | 4.185 | 4.309 |

| Energy Mev | | W1 | W2 | W3 | W4 | W5 | W6 | W7 | W8 | W9 | W10 |
|---|---|---|---|---|---|---|---|---|---|---|---|
| 3.47E-01 | $^{(60)}$Co | 3.913 | 3.889 | 3.983 | 4.125 | 4.126 | 3.912 | 3.935 | 3.936 | 4.125 | 4.247 |
| 3.56E-01 | $^{(133)}$Ba | 3.744 | 3.722 | 3.811 | 3.946 | 3.947 | 3.744 | 3.766 | 3.767 | 3.946 | 4.061 |
| 3.65E-01 | $^{(131)}$I | 3.597 | 3.575 | 3.660 | 3.789 | 3.789 | 3.596 | 3.617 | 3.618 | 3.789 | 3.898 |
| 3.84E-01 | $^{(133)}$Ba | 3.301 | 3.280 | 3.358 | 3.473 | 3.474 | 3.300 | 3.319 | 3.320 | 3.474 | 3.572 |
| 4.00E-01 | | 3.091 | 3.072 | 3.143 | 3.250 | 3.251 | 3.090 | 3.108 | 3.109 | 3.250 | 3.340 |
| 4.11E-01 | $^{(152)}$Eu | 2.962 | 2.944 | 3.012 | 3.113 | 3.114 | 2.961 | 2.978 | 2.979 | 3.113 | 3.198 |
| 4.44E-01 | $^{(152)}$Eu | 2.640 | 2.624 | 2.684 | 2.771 | 2.772 | 2.640 | 2.655 | 2.656 | 2.771 | 2.845 |
| 5.00E-01 | | 2.242 | 2.228 | 2.277 | 2.348 | 2.348 | 2.241 | 2.253 | 2.255 | 2.348 | 2.407 |
| 5.11E-01 | $^{(22)}$Na | 2.179 | 2.166 | 2.213 | 2.282 | 2.282 | 2.178 | 2.191 | 2.192 | 2.281 | 2.338 |
| 6.00E-01 | | 1.795 | 1.784 | 1.822 | 1.875 | 1.875 | 1.795 | 1.805 | 1.806 | 1.874 | 1.918 |
| 6.37E-01 | $^{(131)}$I | 1.681 | 1.671 | 1.705 | 1.754 | 1.754 | 1.680 | 1.689 | 1.690 | 1.753 | 1.793 |
| 6.62E-01 | $^{(137)}$Cs | 1.615 | 1.605 | 1.637 | 1.683 | 1.684 | 1.614 | 1.623 | 1.624 | 1.683 | 1.720 |
| 6.78E-01 | $^{(152)}$Eu | 1.574 | 1.565 | 1.597 | 1.641 | 1.641 | 1.573 | 1.582 | 1.583 | 1.641 | 1.677 |
| 6.89E-01 | $^{(152)}$Eu | 1.549 | 1.540 | 1.571 | 1.615 | 1.615 | 1.549 | 1.557 | 1.558 | 1.614 | 1.649 |
| 7.23E-01 | $^{(131)}$I | 1.476 | 1.467 | 1.497 | 1.538 | 1.538 | 1.475 | 1.484 | 1.485 | 1.537 | 1.570 |
| 7.79E-01 | $^{(152)}$Eu | 1.376 | 1.367 | 1.394 | 1.431 | 1.432 | 1.375 | 1.382 | 1.383 | 1.431 | 1.460 |
| 8.00E-01 | | 1.342 | 1.334 | 1.360 | 1.396 | 1.397 | 1.341 | 1.349 | 1.350 | 1.396 | 1.424 |
| 8.26E-01 | $^{(60)}$Co | 1.304 | 1.296 | 1.322 | 1.356 | 1.356 | 1.303 | 1.311 | 1.312 | 1.356 | 1.383 |
| 8.67E-01 | $^{(152)}$Eu | 1.250 | 1.242 | 1.266 | 1.299 | 1.299 | 1.249 | 1.256 | 1.257 | 1.298 | 1.324 |
| 9.64E-01 | $^{(152)}$Eu | 1.144 | 1.137 | 1.158 | 1.187 | 1.187 | 1.143 | 1.149 | 1.150 | 1.187 | 1.209 |
| 1.00E+00 | | 1.110 | 1.103 | 1.124 | 1.152 | 1.152 | 1.109 | 1.115 | 1.116 | 1.151 | 1.173 |
| 1.01E+00 | $^{(152)}$Eu | 1.105 | 1.098 | 1.119 | 1.147 | 1.147 | 1.104 | 1.110 | 1.111 | 1.146 | 1.168 |
| 1.09E+00 | $^{(152)}$Eu | 1.039 | 1.033 | 1.052 | 1.078 | 1.078 | 1.038 | 1.044 | 1.045 | 1.077 | 1.097 |
| 1.09E+00 | $^{(152)}$Eu | 1.036 | 1.030 | 1.049 | 1.074 | 1.075 | 1.035 | 1.041 | 1.042 | 1.074 | 1.094 |
| 1.11E+00 | $^{(152)}$Eu | 1.021 | 1.014 | 1.033 | 1.058 | 1.058 | 1.020 | 1.025 | 1.026 | 1.058 | 1.077 |
| 1.17E+00 | $^{(60)}$Co | 0.982 | 0.976 | 0.994 | 1.018 | 1.018 | 0.981 | 0.986 | 0.987 | 1.017 | 1.035 |
| 1.28E+00 | $^{(22)}$Na | 0.928 | 0.923 | 0.939 | 0.962 | 0.962 | 0.927 | 0.933 | 0.933 | 0.961 | 0.978 |
| 1.30E+00 | $^{(152)}$Eu | 0.917 | 0.912 | 0.928 | 0.950 | 0.950 | 0.917 | 0.922 | 0.922 | 0.950 | 0.967 |
| 1.33E+00 | $^{(60)}$Co | 0.903 | 0.897 | 0.914 | 0.935 | 0.935 | 0.902 | 0.907 | 0.908 | 0.935 | 0.951 |
| 1.41E+00 | $^{(152)}$Eu | 0.874 | 0.869 | 0.885 | 0.905 | 0.905 | 0.873 | 0.878 | 0.879 | 0.905 | 0.921 |
| 1.46E+00 | $^{(152)}$Eu | 0.857 | 0.852 | 0.868 | 0.888 | 0.888 | 0.857 | 0.861 | 0.862 | 0.887 | 0.903 |
| 1.50E+00 | | 0.845 | 0.839 | 0.855 | 0.874 | 0.875 | 0.844 | 0.848 | 0.849 | 0.874 | 0.889 |
| 2.00E+00 | | 0.748 | 0.743 | 0.757 | 0.775 | 0.775 | 0.747 | 0.751 | 0.752 | 0.774 | 0.788 |
| 2.51E+00 | $^{(60)}$Co | 0.704 | 0.699 | 0.712 | 0.730 | 0.730 | 0.703 | 0.707 | 0.708 | 0.729 | 0.743 |
| 3.00E+00 | | 0.682 | 0.678 | 0.691 | 0.708 | 0.709 | 0.682 | 0.686 | 0.686 | 0.708 | 0.722 |
| 4.00E+00 | | 0.672 | 0.667 | 0.681 | 0.699 | 0.699 | 0.671 | 0.675 | 0.676 | 0.699 | 0.713 |
| 5.00E+00 | | 0.679 | 0.675 | 0.688 | 0.707 | 0.708 | 0.679 | 0.683 | 0.683 | 0.708 | 0.723 |
| 6.00E+00 | | 0.694 | 0.690 | 0.704 | 0.724 | 0.724 | 0.694 | 0.698 | 0.698 | 0.724 | 0.740 |
| 8.00E+00 | | 0.733 | 0.728 | 0.744 | 0.766 | 0.766 | 0.733 | 0.737 | 0.738 | 0.766 | 0.784 |
| 1.00E+01 | | 0.775 | 0.770 | 0.787 | 0.811 | 0.811 | 0.775 | 0.780 | 0.780 | 0.811 | 0.831 |
| 1.50E+01 | | 0.874 | 0.868 | 0.888 | 0.916 | 0.916 | 0.875 | 0.880 | 0.880 | 0.917 | 0.940 |

**Table (4):** LAC results of each alloy calculated via the online MATXCOM software.

| Energy, MeV | W1 | W2 | W3 | W4 | W5 | W6 | W7 | W8 | W9 | W10 |
|---|---|---|---|---|---|---|---|---|---|---|
| 1.50E-02 | 2215.38 | 2199.96 | 2253.11 | 2329.38 | 2331.80 | 2224.53 | 2238.24 | 2237.15 | 2338.30 | 2401.78 |
| 2.00E-02 | 1052.04 | 1044.72 | 1070.23 | 1107.00 | 1108.15 | 1056.42 | 1062.94 | 1062.40 | 1111.26 | 1141.97 |
| 3.00E-02 | 362.27 | 359.77 | 368.68 | 381.63 | 382.01 | 363.76 | 366.01 | 365.82 | 383.07 | 393.94 |
| 4.00E-02 | 169.12 | 167.96 | 172.15 | 178.29 | 178.46 | 169.79 | 170.84 | 170.75 | 178.94 | 184.10 |
| 5.00E-02 | 93.63 | 92.98 | 95.32 | 98.74 | 98.83 | 93.98 | 94.56 | 94.51 | 99.09 | 101.98 |
| 6.00E-02 | 57.83 | 57.44 | 58.88 | 61.00 | 61.06 | 58.04 | 58.40 | 58.37 | 61.21 | 63.00 |
| 8.00E-02 | 120.22 | 119.48 | 122.85 | 128.21 | 128.23 | 120.31 | 121.02 | 121.01 | 128.30 | 133.02 |
| 1.00E-01 | 68.27 | 67.86 | 69.76 | 72.79 | 72.81 | 68.32 | 68.72 | 68.72 | 72.84 | 75.51 |
| 1.50E-01 | 24.46 | 24.31 | 24.98 | 26.05 | 26.05 | 24.48 | 24.62 | 24.62 | 26.06 | 26.99 |
| 2.00E-01 | 12.23 | 12.15 | 12.48 | 12.99 | 12.99 | 12.23 | 12.30 | 12.30 | 13.00 | 13.44 |
| 3.00E-01 | 5.12 | 5.09 | 5.22 | 5.41 | 5.41 | 5.12 | 5.15 | 5.15 | 5.41 | 5.58 |

| | | | | | | | | | | |
|---|---|---|---|---|---|---|---|---|---|---|
| 4.00E-01 | 3.09 | 3.07 | 3.14 | 3.25 | 3.25 | 3.09 | 3.11 | 3.11 | 3.25 | 3.34 |
| 5.00E-01 | 2.24 | 2.23 | 2.28 | 2.35 | 2.35 | 2.24 | 2.25 | 2.25 | 2.35 | 2.41 |
| 6.00E-01 | 1.79 | 1.78 | 1.82 | 1.87 | 1.87 | 1.79 | 1.80 | 1.80 | 1.87 | 1.92 |
| 8.00E-01 | 1.34 | 1.33 | 1.36 | 1.39 | 1.39 | 1.34 | 1.34 | 1.35 | 1.39 | 1.42 |
| 1.00E+00 | 1.11 | 1.10 | 1.12 | 1.15 | 1.15 | 1.11 | 1.11 | 1.11 | 1.15 | 1.17 |
| 1.50E+00 | 0.84 | 0.84 | 0.85 | 0.87 | 0.87 | 0.84 | 0.85 | 0.85 | 0.87 | 0.89 |
| 2.00E+00 | 0.75 | 0.74 | 0.75 | 0.77 | 0.77 | 0.75 | 0.75 | 0.75 | 0.77 | 0.79 |
| 3.00E+00 | 0.68 | 0.68 | 0.69 | 0.71 | 0.71 | 0.68 | 0.68 | 0.69 | 0.71 | 0.72 |
| 4.00E+00 | 0.67 | 0.67 | 0.68 | 0.70 | 0.70 | 0.67 | 0.67 | 0.67 | 0.70 | 0.71 |
| 5.00E+00 | 0.68 | 0.67 | 0.69 | 0.71 | 0.71 | 0.68 | 0.68 | 0.68 | 0.71 | 0.72 |
| 6.00E+00 | 0.69 | 0.69 | 0.70 | 0.72 | 0.72 | 0.69 | 0.70 | 0.70 | 0.72 | 0.74 |
| 8.00E+00 | 0.73 | 0.73 | 0.74 | 0.76 | 0.77 | 0.73 | 0.74 | 0.74 | 0.77 | 0.78 |
| 1.00E+01 | 0.77 | 0.77 | 0.79 | 0.81 | 0.81 | 0.77 | 0.78 | 0.78 | 0.81 | 0.83 |
| 1.50E+01 | 0.87 | 0.87 | 0.89 | 0.92 | 0.92 | 0.87 | 0.88 | 0.88 | 0.92 | 0.94 |

**Table (5):** LAC results of each alloy according to the NGCal calculations.

| Sample ID | Linear attenuation factor. cm $^{-1}$ | | Linear attenuation coefficient. cm $^{-1}$ | | |
|---|---|---|---|---|---|
| | Neutrons | | Photons | | |
| | Thermal (25.4 meV) | Fast (4 MeV) | 0.00589 MeV | 1 MeV | 15 MeV |
| W1 | 1.12679534604015 | 0.146567549262489 | 5777.78673753182 | 1.10986525 | 0.87385844 |
| W2 | 1.10878222833654 | 0.127461492812684 | 5739. 33211949184 | 1.10302084 | 0.86830464 |
| W3 | 1.13429278469541 | 0.140092195909779 | 5889.48206257145 | 1.12378293 | 0.88772942 |
| W4 | 1.14887801867179 | 0.126565357235032 | 6115.91265304588 | 1.15167325 | 0.91571933 |
| W5 | 1.16069124275872 | 0.135147433114929 | 6120.35695599971 | 1.15196265 | 0.91611844 |
| W6 | 1.12154963914592 | 0.138887397942826 | 5795.34400327935 | 1.10895096 | 0.87452092 |
| W7 | 1.11826006334917 | 0.131525162581132 | 5830.81327620153 | 1.11507256 | 0.87957151 |
| W8 | 1.25856714750762 | 0.391176910987682 | 4007.55168476637 | 1.07712894 | 0.72864684 |
| W9 | 1.15366397798035 | 0.127037299584565 | 6132.88133073084 | 1.15117975 | 0.91653275 |
| W10 | 1.17168139089224 | 0.120692353023867 | 6326.96863888427 | 1.17300576 | 0.93972252 |

## 4. Results and Discussion

Given the peaceful uses of radiation or neutrons, currently employed in many scientific fields, particularly nuclear science, medicine, and others, it has become essential to provide means of shielding radiation to safe levels for workers in these fields and protecting them from its dangers. This protection is achieved by using materials with suitable radiation shielding properties. Various alloys, depending on tungsten as a preferred metal over heavy metals such as lead, due to its superior radiation shielding properties, were tested [18-21].

In this study, ten alloys containing tungsten with significantly higher percentages than iron, nickel, and copper were tested via Phy -X, MATXCOM, and NGCal software.

The linear attenuation coefficient depends on density (**ρ**) and mean atomic number ($\bar{\mathbf{Z}}$). The increasing sequence of density is W2,( W1, W6),( W7, W8) , W3, (W4, W5, W9), W10 that rises the probability of absorption or scattering whereas the $\bar{\mathbf{Z}}$ is W2, W1, W8, W6, W7, W3, W4, W5, W9, and W10.

Depending on how radiation or neutron interacts with matter, the increase in the ($\bar{\mathbf{Z}}$) refers to the increase in collisions with electrons or interactions with the nucleus, thus resulting in greater attenuation. Photon, charged particle, or neutron has its own interaction mechanism (Figures 1 & 2) with matter where the increase in the ($\bar{\mathbf{Z}}$) increases the probability of photoelectric absorption, Compton scattering, and pair production (in the case of the photon (Gamma rays or X-rays)) via increasing the density of orbital electrons that leads to higher rate of ionization or excitation (in the of the charged particles (electron, α, or ion)) leading to loss of collision energy. In the case of a neutron, the increase of the ($\bar{\mathbf{Z}}$) affects the neutron interaction cross –section whether this neutron is moderated by material (low $\bar{\mathbf{Z}}$) or scattered/absorbed (high $\bar{\mathbf{Z}}$). Overall, the ($\bar{\mathbf{Z}}$) controls the LAC and other related attenuation factors [22 - 25]. In this theoretical study, three free computerized models were chosen to calculate the LAC

parameter to evaluate the attenuation behavior of ten refectory alloys against gamma rays, X-rays, and neutron exposure. Tables (2-5) show the theoretical performance of these alloys.

Tables (6-9) and Figures (3-6) respectively display the difference of error (Δ%**)** for the linear attenuation coefficient of ten alloys between the tested models. This calculation is based on equation (1) and confirms that these models are suitable for this theoretical study, where Δ% data were low and within internationally accepted differences.

The (**Δ%)** calculations indicate the accuracy and reliability of all obtained LAC (μ, $cm^{-1}$) via the three models [26, 27].

$$\Delta\% = (\mu_{Phy\text{-}X} - \mu_{NGCal})/\mu_{Phys\text{-}X}) \times 100 \qquad (1)$$

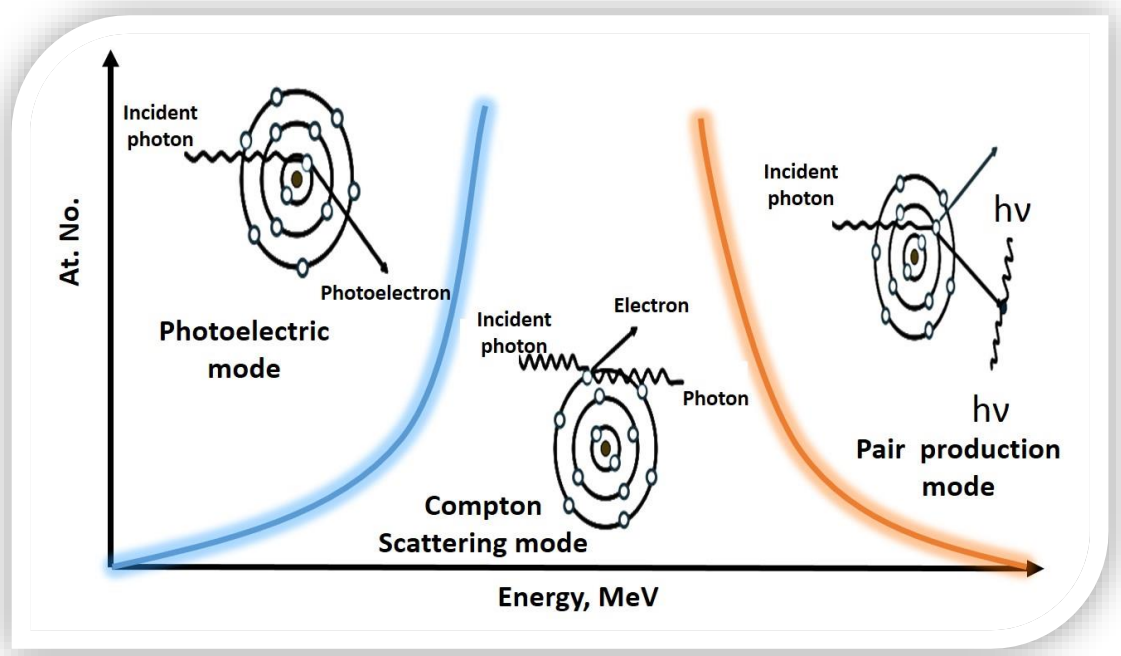


**Figure (1).** Photon interaction modes with matter.

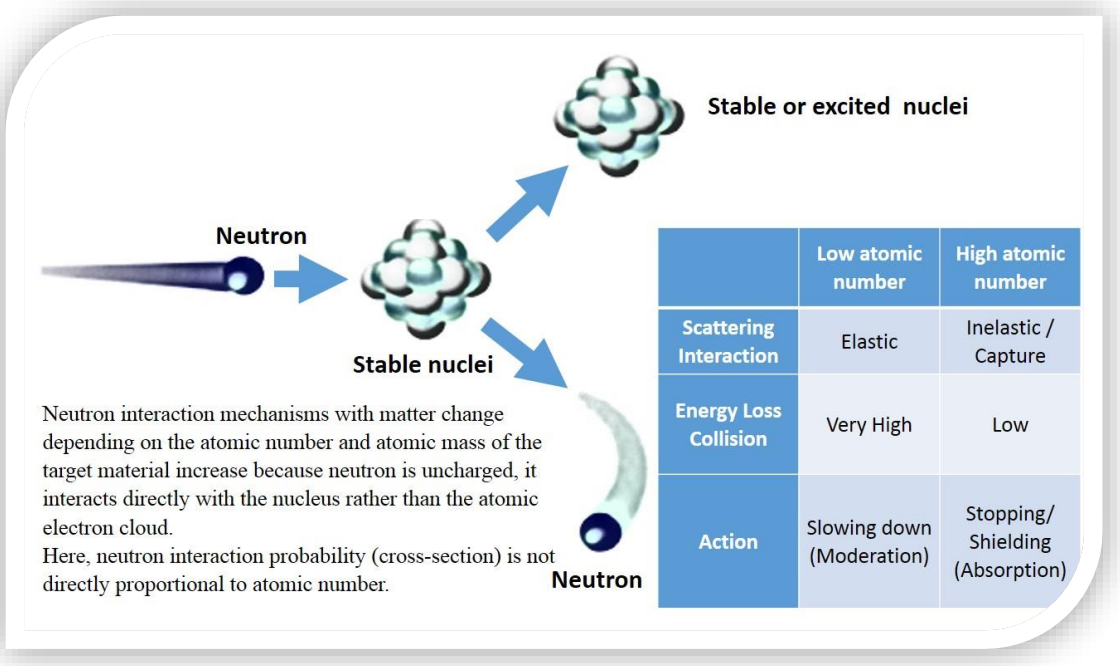


**Figure (2).** Neutron interaction modes with matter.

**Table (6):** The difference of error results Phy- and NGCal software in the case of photon exposure.

| Code | Phy-X | | | NGCal | | | Error, % | | |
|---|---|---|---|---|---|---|---|---|---|
| | 5.89E-03 MeV | 1 MeV | 15 MeV | 5.89E-03 MeV | 1 MeV | 15 MeV | 5.89E-03 MeV | 1MeV | 15 MeV |
| W1 | 5780.837 | 1.110 | 0.874 | 5777.787 | 1.109865 | 0.873858 | 0.052765 | 0.012147 | 0.016197 |
| W2 | 5742.365 | 1.103 | 0.868 | 5602.681 | 1.103020 | 0.868304 | 0.052816 | -0.001885 | -0.035023 |
| W3 | 5892.588 | 1.124 | 0.888 | 5889.482 | 1.123783 | 0.887729 | 0.052709 | 0.019312 | 0.030473 |
| W4 | 6119.132 | 1.152 | 0.916 | 6115.913 | 1.151673 | 0.915719 | 0.052611 | 0.028364 | 0.030677 |
| W5 | 6123.575 | 1.152 | 0.916 | 6120.357 | 1.151962 | 0.916118 | 0.052552 | 0.003299 | -0.012885 |
| W6 | 5798.417 | 1.109 | 0.875 | 5795.344 | 1.108951 | 0.916118 | 0.052997 | 0.004422 | 0.054752 |
| W7 | 5833.911 | 1.115 | 0.883 | 5830.813 | 1.115073 | 0.879572 | 0.053099 | -0.006565 | 0.048693 |
| W8 | 5831.544 | 1.116 | 0.881 | 5828.459 | 1.115953 | 0.879813 | 0.052907 | 0.004203 | 0.113636 |
| W9 | 6136.118 | 1.151 | 0.917 | 6132.881 | 1.151182 | 0.916533 | 0.052748 | -0.015624 | 0.050954 |
| W10 | 6330.295 | 1.173 | 0.943 | 6326.969 | 1.173006 | 0.939723 | 0.052547 | -0.000494 | 0.029519 |

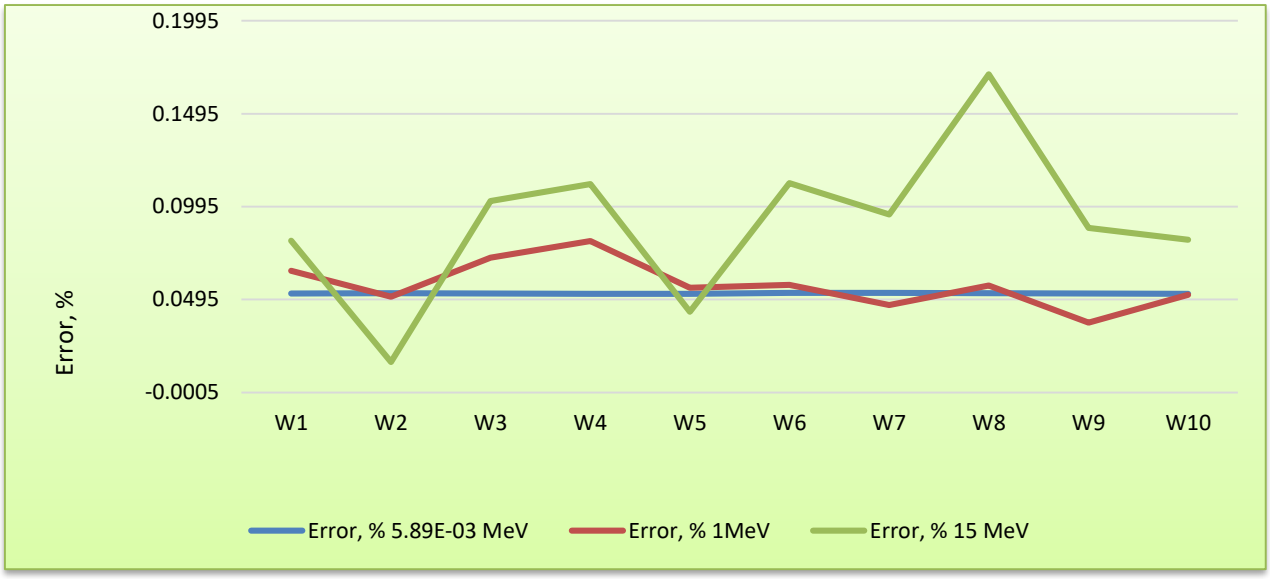


**Figure (3):** The difference of error results for energies (0.00589, 1, 15) MeV.

**Table (7)**: The difference of error results MATXCOM and NGCal software.

| Code | MATXCOM | | NGCal | | Error, % | |
|---|---|---|---|---|---|---|
| | 1 MeV | 15 MeV | 1 MeV | 15 MeV | 1 MeV | 15 MeV |
| W1 | 1.10604 | 0.87334 | 1.109865 | 0.873858 | -0.34585 | -0.05936 |
| W2 | 1.09922 | 0.86779 | 1.103048 | 0.868375 | -0.34574 | -0.05877 |
| W3 | 1.11989 | 0.88721 | 1.123782 | 0.887729 | -0.34762 | -0.05854 |
| W4 | 1.14764 | 0.91519 | 1.151673 | 0.915716 | -0.35144 | -0.0578 |
| W5 | 1.14792 | 0.91559 | 1.151962 | 0.916118 | -0.35212 | -0.05767 |
| W6 | 1.10512 | 0.87427 | 1.108951 | 0.874520 | -0.34666 | -0.0596 |
| W7 | 1.11122 | 0.87905 | 1.115072 | 0.879571 | -0.34669 | -0.05933 |
| W8 | 1.11213 | 0.8793 | 1.115953 | 0.879819 | -0.34647 | -0.05902 |
| W9 | 1.14714 | 0.91601 | 1.151179 | 0.916532 | -0.35216 | -0.05707 |
| W10 | 1.16885 | 0.93919 | 1.173005 | 0.939722 | -0.35554 | -0.05675 |

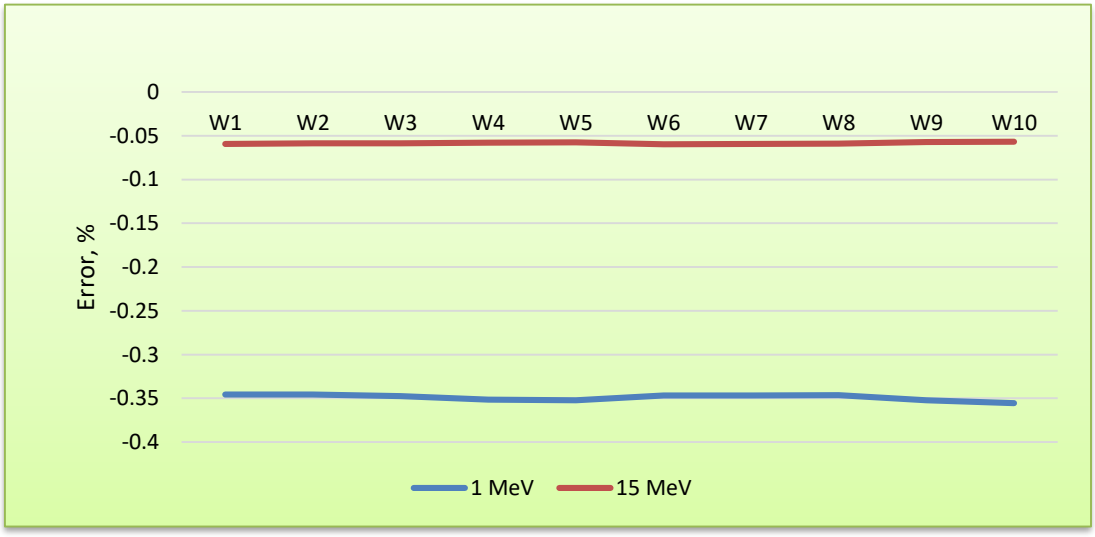


**Figure (4):** The difference of error results for energies (1, 15) MeV.

**Table (8):** The difference of error Phy-X and MATXCOM software.

| Code | Isotope Phy-X | | | standard MATXCOM | | | Error, % | | |
|---|---|---|---|---|---|---|---|---|---|
| | 1.50E-02 Mev | 1Mev | 15 Mev | 1.50E-02 Mev | 1 Mev | 15Mev | 1.50E-02 Mev | 1 Mev | 15 Mev |
| W1 | 2225.140 | 1.110 | 0.874 | 2215.383 | 1.106 | 0.873 | 0.439 | 0.357 | 0.076 |
| W2 | 2209.668 | 1.103 | 0.868 | 2199.956 | 1.099 | 0.868 | 0.439 | 0.342 | 0.024 |
| W3 | 2263.114 | 1.124 | 0.888 | 2253.114 | 1.120 | 0.887 | 0.442 | 0.366 | 0.089 |
| W4 | 2263.114 | 1.152 | 0.916 | 2329.383 | 1.148 | 0.915 | 0.449 | 0.379 | 0.089 |
| W5 | 2342.280 | 1.152 | 0.916 | 2331.796 | 1.148 | 0.916 | 0.448 | 0.345 | 0.045 |
| W6 | 2234.291 | 1.109 | 0.875 | 2224.532 | 1.105 | 0.974 | 0.437 | 0.351 | 0.114 |
| W7 | 2248.063 | 1.115 | 0.880 | 2238.238 | 1.111 | 0.879 | 0.437 | 0.339 | 0.108 |
| W8 | 2246.961 | 1.116 | 0.880 | 2237.152 | 1.112 | 0.879 | 0.437 | 0.349 | 0.079 |
| W9 | 2348.786 | 1.151 | 0.917 | 2338.28 | 1.147 | 0.916 | 0.447 | 0.335 | 0.079 |
| W10 | 2412.708 | 1.173 | 0.940 | 2401.783 | 1.169 | 0.940 | 0.453 | 0.359 | 0.086 |

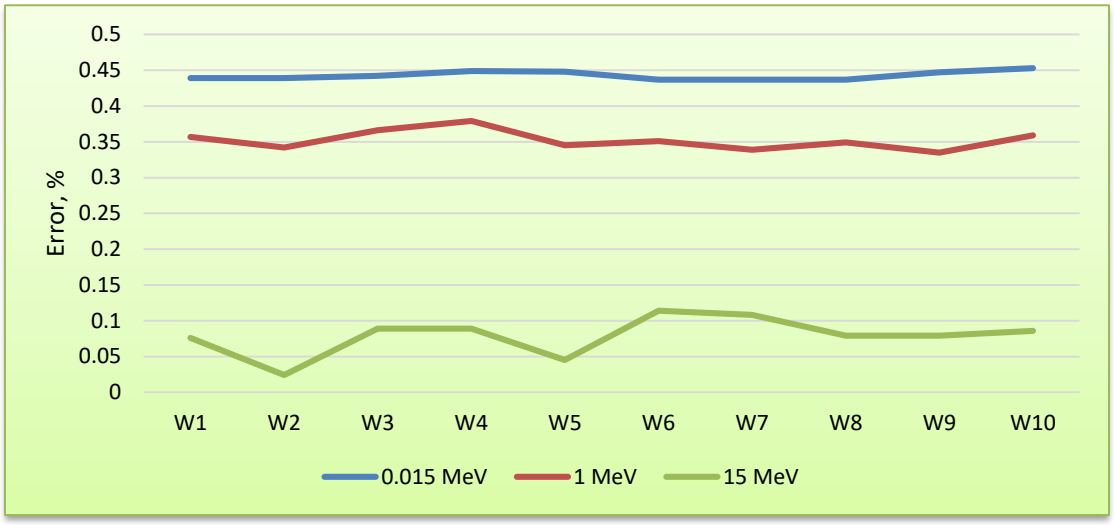


**Figure (5):** The difference of error results for energies (0.015, 1, 15) MeV.

**Table (9):** The difference of error results Phy-X and MATXCOM software in the case of the X-rays attenuation.

| Code | PHY-X | | | | MATXCOM | | | | Error, % | | | |
|---|---|---|---|---|---|---|---|---|---|---|---|---|
| | $_{29}$Cu | | $_{37}$Rb | | $_{29}$Cu | | $_{37}$Rb | | $_{29}$Cu | | $_{37}$Rb | |
| | 8.04E-03 Mev | 8.91E-03 Mev | 1.34E-02 Mev | 1.50E-02 Mev | 8.04E-03 Mev | 8.91E-03 Mev | 1.34E-02 Mev | 1.50E-02 Mev | 8.04E-03 Mev | 8.91E-03 Mev | 1.34E-02 Mev | 1.50E-02 Mev |
| W1 | 2771.651 | 2420.777 | 2973.405 | 2236.388 | 2755.287 | 2404.4334 | 2970.714 | 2226.825 | 0.5903 | 0.6751 | 0.0905 | 0.42758 |
| W2 | 2797.745 | 2398.544 | 2952.667 | 2220.837 | 2781.452 | 2381.9648 | 2950.022 | 2211.324 | 0.5823 | 0.6893 | 0.0895 | 0.42833 |
| W3 | 2824.888 | 2423.882 | 3023.725 | 2274.548 | 2808.275 | 2407.0366 | 3020.990 | 2264.749 | 0.5880 | 0.6948 | 0.0904 | 0.43079 |
| W4 | 2940.702 | 2428.294 | 3125.425 | 2351.688 | 2915.681 | 2410.4287 | 3122.604 | 2341.408 | 0.8508 | 0.7357 | 0.0902 | 0.43712 |
| W5 | 2888.531 | 2436.583 | 3128.701 | 2354.103 | 2871.444 | 2419.0134 | 3125.848 | 2343.830 | 0.5915 | 0.7209 | 0.0911 | 0.43638 |
| W6 | 2645.424 | 2282.537 | 2985.958 | 2245.588 | 2629.311 | 2266.0637 | 2982.870 | 2236.014 | 0.6090 | 0.7217 | 0.1034 | 0.42631 |
| W7 | 2661.585 | 2255.243 | 3004.397 | 2259.434 | 2644.319 | 2238.4207 | 3001.214 | 2249.792 | 0.6486 | 0.7459 | 0.1059 | 0.42655 |
| W8 | 2660.569 | 2336.843 | 3002.856 | 2258.321 | 2644.319 | 2320.524 | 2999.826 | 2248.699 | 0.6107 | 0.6983 | 0.1008 | 0.42606 |
| W9 | 2801.568 | 2327.147 | 3137.631 | 2360.644 | 2784.667 | 2309.4055 | 3134.478 | 2350.361 | 0.6032 | 0.7623 | 0.1004 | 0.43558 |
| W10 | 2891.611 | 2356.581 | 3222.113 | 2424.877 | 2874.259 | 2338.1589 | 3218.964 | 2414.169 | 0.6000 | 0.7817 | 0.0977 | 0.44156 |

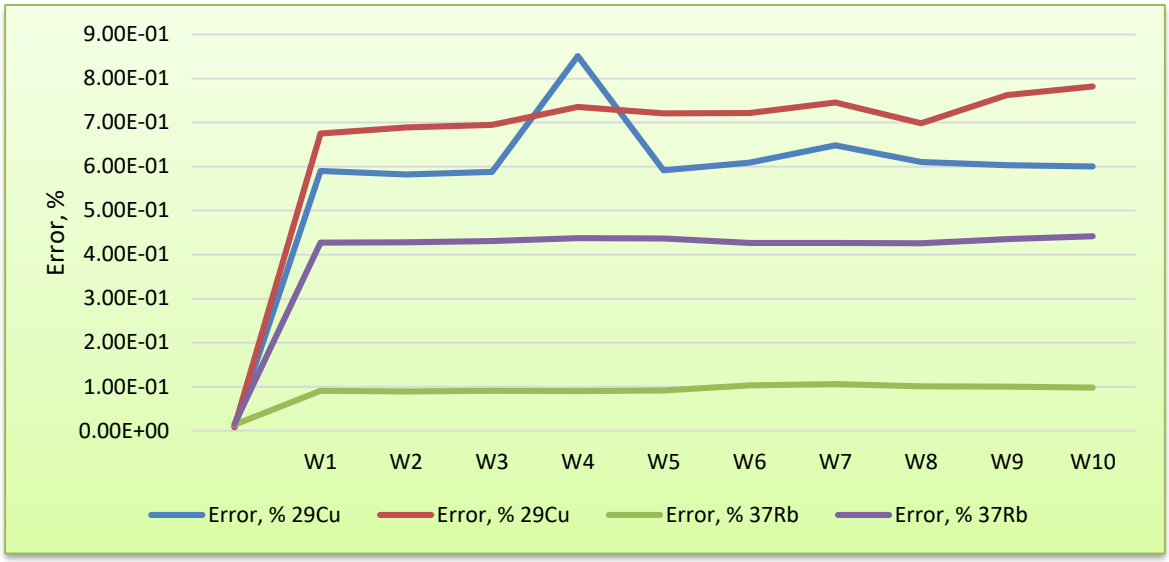


**Figure (6):** The difference of error results for energies (0.00804, 0.00891, 0.0134, 0.015) MeV.

From Tables (2-5), W1 and W8 contain the same percentage of tungsten and nickel, but they differ in the third element (Fe and Cu), respectively. However, copper has a higher density and a higher atomic number (Figure 7), and for these important reasons, W8 is the best alloy for attenuation, especially at high energy exposure. The 90W-7Ni-3Fe and 90W-7Ni-3Cu alloys are both heavy alloys of two phases consisting of 90% tungsten with a binder matrix: Ni-Fe and Ni-Cu, respectively, that reflects their microstructures and related properties. They consist of spherical W in a ductile matrix [28, 29].

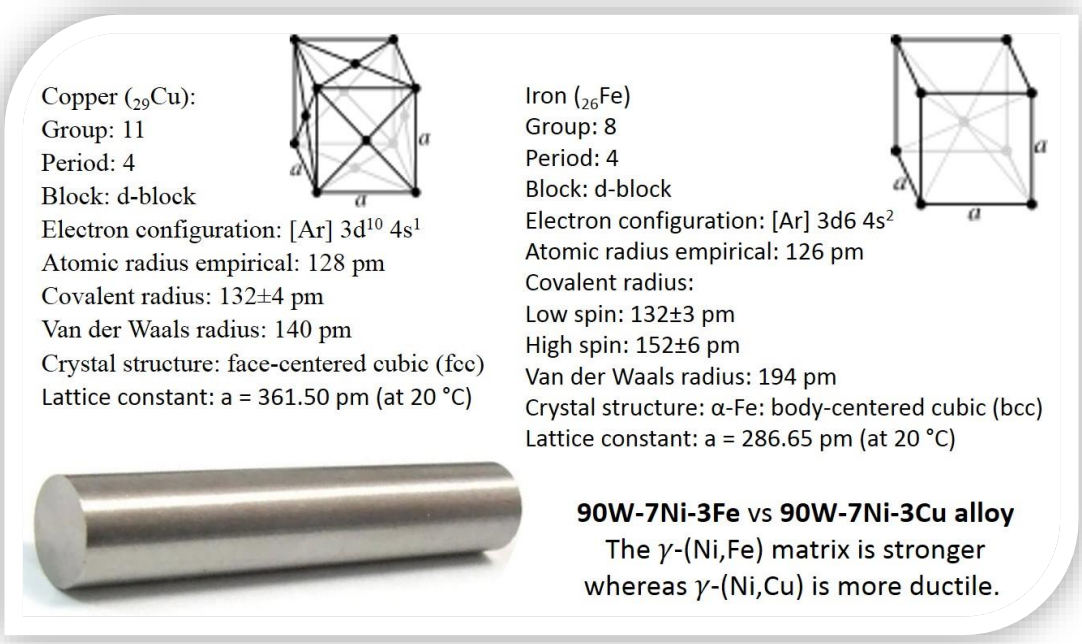


**Figure (7):** Copper and Iron structural properties.

The calculated results showed that the best alloy for absorbing gamma rays and X-rays is the 95W-3Ni-2Cu alloy, which is preferred over the tested alloys for shielding purposes because it contains the highest percentage of tungsten, which has a high density and atomic number among all the basic elements in these alloys. The increasing

of the interaction probability during the exposure leads to high attenuation with a small thickness in addition to its good mechanical properties (Table 1).

In general, the linear attenuation coefficient (LAC) depends on the density, energy of the radiation, chemical composition, and atomic number of the materials. This coefficient is a fundamental parameter in attenuation calculations and is directly proportional to the density, mainly depending on the Lambert–Beer (equation (2)). In general, the linear attenuation coefficient decreased with increasing energy [30].

$$\mathbf{I = I_0 e^{-\mu x}} \qquad \mathbf{(2)}$$

Where: **μ**: Linear Attenuation Coefficient, $\mathbf{I_o}$: intensity of the incident photon, **I**: transmitted photons through the material, and **x**: thickness (cm).

The results obtained from the models provide detailed and accurate attenuation parameters (Tables 2-5). Table (2) shows LAC results that were calculated via Phy-X software for X-ray exposure from $_{29}$Cu, $_{37}$Rb, $_{42}$Mo, $_{47}$Ag, $_{56}$Ba, and $_{65}$Tb at (0.00804-15) MeV, decreased with increasing energy, and represent the **W2** alloy and **W10** alloy as the lowest and highest attenuation materials under testing, respectively.

Table (3) displays LAC, which was calculated via Phy-X software for gamma ray exposure that may be emitted from many isotopes in their energy range (0.00589-15) MeV. Here, the LAC data are with the same mode as in X-ray exposure.

In comparison, Table (4) shows LAC results of gamma rays exposure that were calculated via the online MATXCOM software at (0.015-15) MeV. The same performance of LAC data has noticed, where LAC was high for low energies and decreased with increasing energy. In addition lowest shielding performance was the **W2** alloy, and the highest was the **W10** alloy.

All X-rays and gamma rays behave with all the tested alloys are based on the probability of the photoelectric effect that depends on the incident photon energy, the electron's binding energy to the shells, the photoelectric absorption edges, as well as the properties of the tested materials. The increase in the photon energy exceeds the binding energy of a particular shell (K, M,), which sharply increases the probability of interaction, where a sharp peak appears in the calculated attenuation coefficient results. At high energies, the electron orbital is much bigger than photon wavelength, changes the electron wave function and decreases the probability of interaction (Figure 1) [31, 32].

The other interaction mechanism is the pair production where the LAC increases slightly and the pair production becomes the dominant process (Figure (1)). The LAC rises again with increasing energy, especially for materials having a high mean atomic number [33, 34].

Table (5) shows the LAC - NGCal for neutron attack with energy [thermal (25.4 meV), fast (4 MeV)] and photon exposure at (0.00589, 1, and 15) MeV. The material interaction with a photon differs from its interaction with a neutron that based on photons, electromagnetic waves without mass, whereas the neutrons are uncharged particles with mass.

For the thermal neutron, the W8 alloy was with highest LAC value, and W2 represents the lowest LAC value.
For the fast neutron, the W8 characterizes the highest LAC value, and lowest attention performance was the [W10] alloy.

The neutron absorption via any materials primarily depends on the percentage of each element and the type of binder (Ni, Cu, and Fe). The 90W-7Ni-3Cu alloy is a superior alloy because it contains a high percentage of tungsten and nickel, which increases the overall absorption cross-section and attenuates both thermal and fast neutrons.

The other calculated parameter is the protection efficiency in terms of the percentage (PE %) (Equation (3), Figures (8-11). Equation (3) is a measure of a material's ability to attenuate and absorb the photons or neutrons, depending on the LAC (**μ**, $cm^{-1}$) data and the thickness (x, cm) [35].

$$PE = (1-(e^{-\mu x})) \times 100 \qquad (3)$$

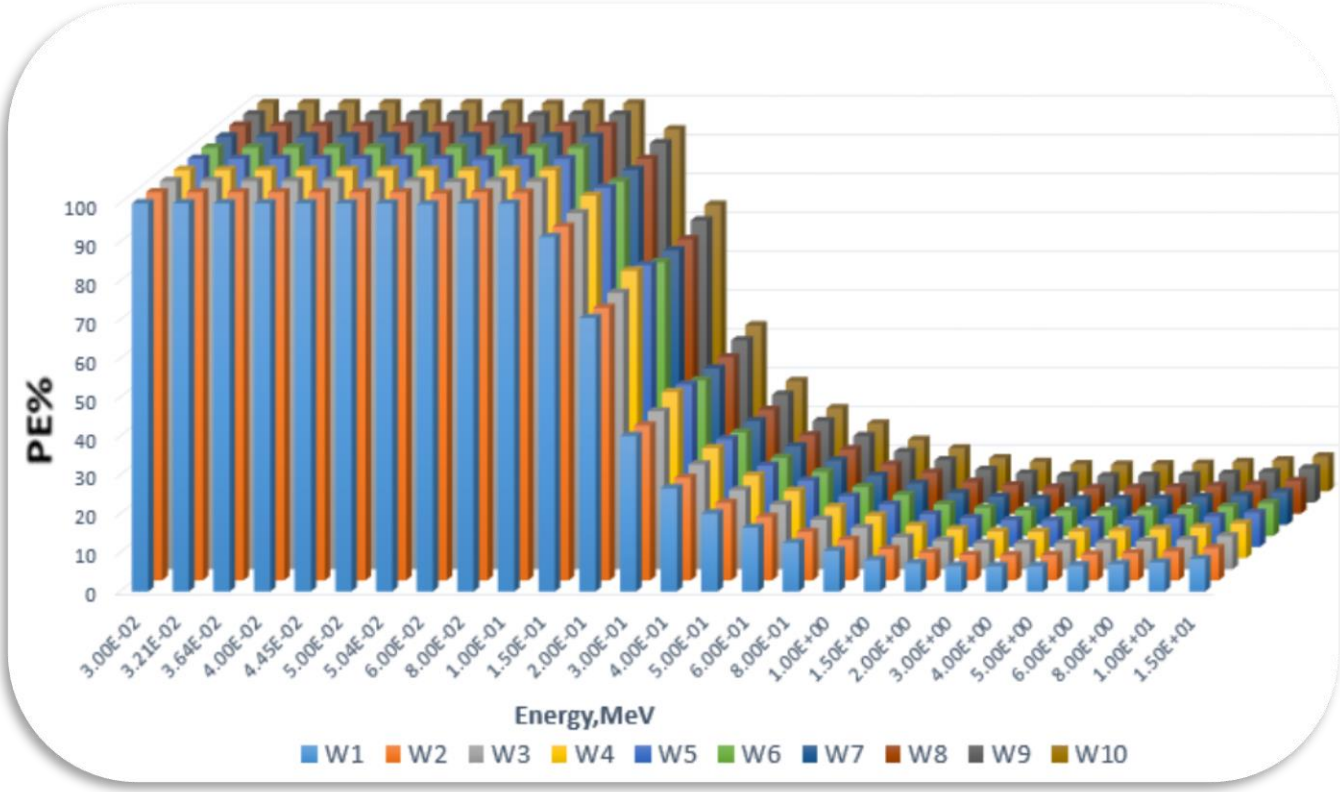


**Figure (8):** The protection efficiency of each alloy with thickness (0.1) cm against X-rays exposure.

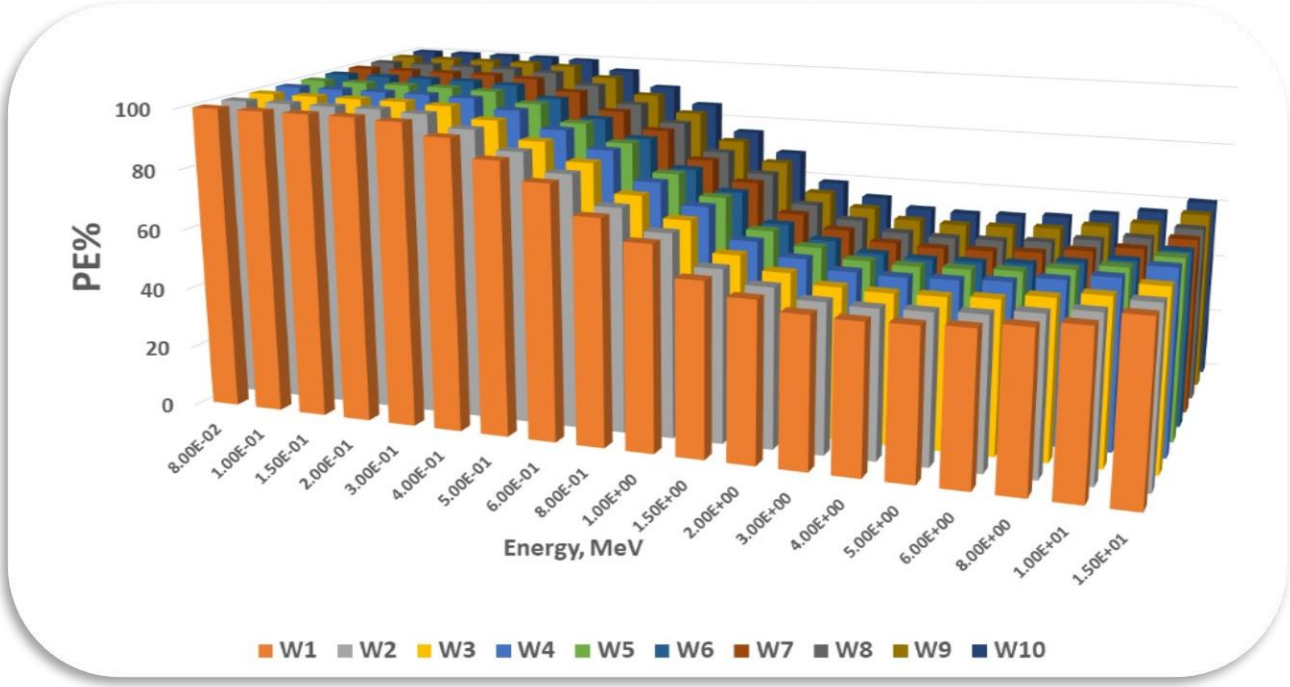


**Figure (9):** The protection efficiency of each alloy with thickness (1) cm against X-rays exposure.

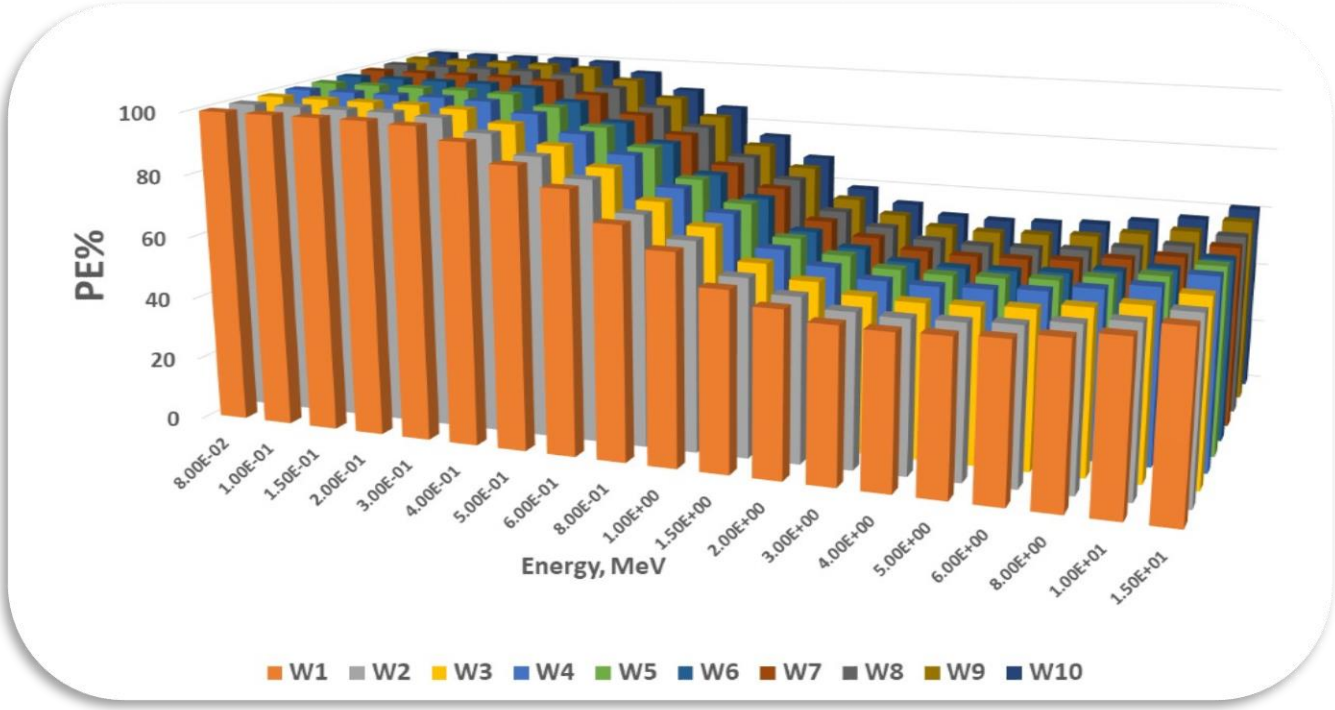


**Figure (10):** The protection efficiency of each alloy with thickness (5) cm against X-rays exposure.

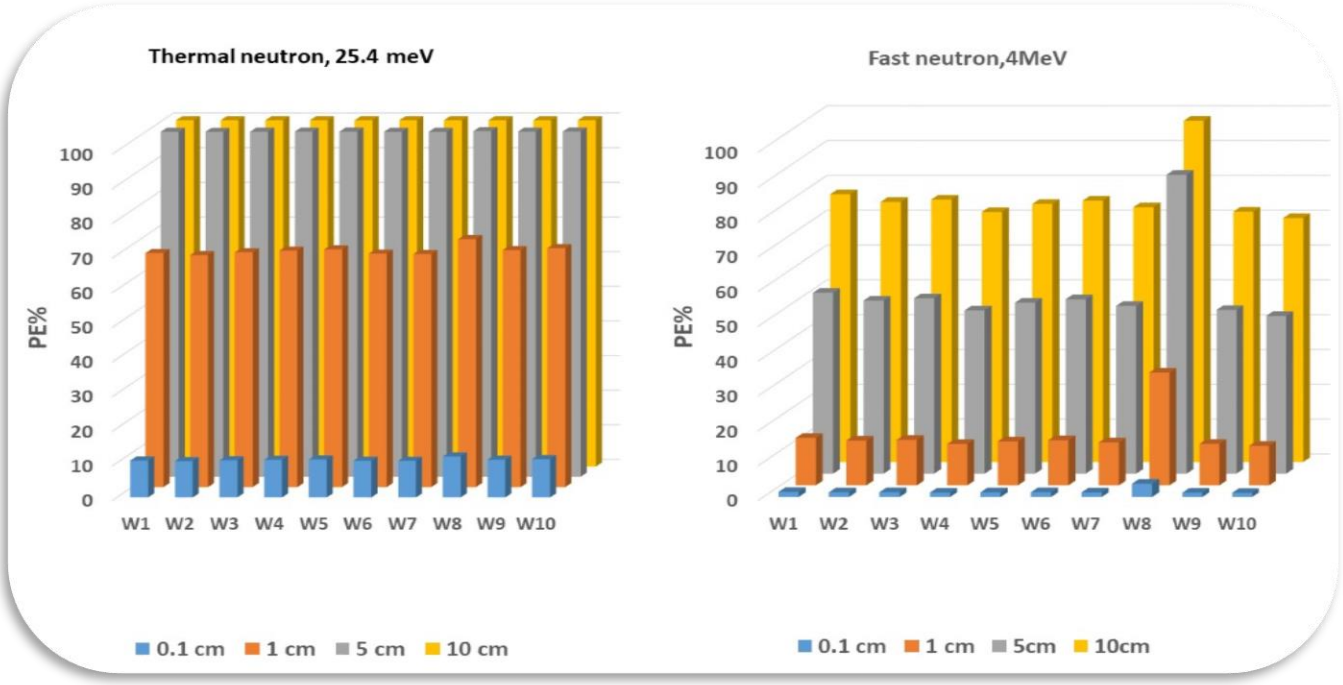


**Figure (11):** The protection efficiency of each alloy with thickness (0.1, 1, 5, and 10) cm against neutron attack.

Figure (11) shows that the protection efficiency of each alloy is higher with thermal neutrons than with fast neutrons because their energies are lower. Additionally, PE% increases with increasing thickness. In conclusion, the superior thermal neutron-attenuating alloy was **W8,** whereas the least effective was **W2**. However, with fast neutrons, the superior alloy was [W8], and the least effective alloy was [W10].

## 5. Conclusions

In this study, three computerized models (Phy-X, MATXCOM, and NGCal) were applied to evaluate the performance of ten refractory alloys against neutron and photon exposures depending on the linear attenuation coefficient (LAC). Different refractory alloys have a high tungsten content compared to the other elements (Ni, Fe, Cu), with high density and mean atomic number. Furthermore, the difference of error (Δ %) between the three models was calculated, and the (Δ%) results were within acceptable limits.

The protection efficiency (PE%) for all the tested alloys at different thicknesses (X) was determined to primarily depend on LAC and X. Based on the obtained results, 95W-3Ni-2Cu alloy proved the most effective for shielding against radiation, whereas 90W-6Ni-4Fe alloy showed the lowest absorption of both X-rays and gamma rays. The 90W-7Ni-3Cu alloy proved to be the best at absorbing neutrons. This study identifies the most effective radiation or neutron shielding alloy that can be safely used.

**Conflict of Interest:** The authors declare that there are no conflicts of interest associated with this research project. We have no financial or personal relationships that could potentially bias our work or influence the interpretation of the results.

## References

[1] S. Ravangvong, K. Sriwongsa, P. Pasuwan, P. Glumglomchit, P. Khunnut, P. Boonchertrong, and I. Huekharnjiraroj, “Simulation radiation shielding properties of tungsten carbide alloys,” *Sci. Eng. Health Stud.*, vol. 19, pp. 1–5, 2025.

[2] M. I. Sayyed, N. Almousa, and M. Elsafi, “Green conversion of the hazardous cathode ray tube and red mud into radiation shielding concrete,” *Materials*, vol. 15, Art. no. 5316, 2022.

[3] N. J. AbuAlRoos, M. N. Azman, N. A. B. Amin, and R. Zainon, “Tungsten-based material as promising new

lead-free gamma radiation shielding material in nuclear medicine," *Phys. Med.*, vol. 78, pp. 48–57, 2020.
[4] G. AlMisned, G. Susoy, D. Sen Baykal, G. Kilic, Ö. Güler, and H. Taken, "Comprehensive performance assessment of Bi- and Pb-based alloys for enhanced gamma-ray and neutron shielding applications," *Radiat. Phys. Chem.*, vol. 237, Art. no. 113006, 2025.
[5] Z. Aygun and M. Aygun, "Radiation shielding potentials of Rene alloys by Phy-X/PSD code," *Acta Phys. Pol. A*, vol. 141, pp. 507–515, 2022.
[6] F. I. El-Agawany, N. Ekinci, K. Mahmoud, S. Sarıtaş, B. Aygün, E. M. Ahmed, and Y. S. Rammah, "Gamma-ray shielding capacity of different B4C-, Re-, and Ni-based superalloys," *Eur. Phys. J. Plus*, vol. 136, Art. no. 527, 2021.
[7] S. Das and S. Dhobi, "Radiation shielding properties of nickel, copper and iron based alloys," *Patan Prospect. J.*, vol. 4, no. 1, pp. 118–134, 2024.
[8] K. Abushahla and H. Arslan, "Lead-free alternatives for radiation shielding in medical environments: A comprehensive review," *J. Sci.*, vol. 29, pp. 602–625, 2025.
[9] J. S. Alzahrani, Z. A. Alrowaili, C. Eke, Z. Mahmoud, C. Mutuwong, and M. S. Al-Buriahi, "Nuclear shielding properties of Ni-, Fe-, Pb-, and W-based alloys," *Radiat. Phys. Chem.*, vol. 195, Art. no. 110090, 2022.
[10] İ. Erkoyuncu, "Gamma/neutron radiation shielding characteristics and produced secondary radiation in Fe-Ni alloys," *J. Alloys Compd.*, vol. 1032, Art. no. 181192, 2025.
[11] K. K. Hammud, "Protection efficiency of various nickel alloys against neutron, gamma radiation and X-rays exposure," *Iraqi J. Ind. Res.*, vol. 12, no. 2, pp. 96–118, 2025.
[12] T. Dewen, L. Xiaoshuang, and X. Weiwei, "Influences of W contents on microstructures, mechanical properties and the shielding performance for neutrons and γ-rays of Fe–W–C alloy," *J. Alloys Compd.*, vol. 827, Art. no. 153932, 2020.
[13] Stanford Materials Corporation, "W-Ni-Fe Alloy," Stanford Materials Corporation. Accessed: Jun. 6, 2026. [Online]. Available: https://www.stanfordmaterials.com/W-Ni-Fe.html
[14] Midwest Tungsten Service, "Tungsten Copper Alloy (W-Cu)," Midwest Tungsten Service. Accessed: Jun. 6, 2026. [Online]. Available: https://www.tungsten.com/material-info/tungsten-copper-alloy-w-cu
[15] E. Şakar, B. Alım, M. I. Sayyed, and M. Kurudirek, "Phy-X/PSD: Development of a user-friendly online software for calculation of parameters relevant to radiation shielding and dosimetry," *Radiat. Phys. Chem.*, vol. 166, Art. no. 108496, 2020.
[16] H. S. Gökçe, O. Güngör, and H. Yılmaz, "An online software to simulate the shielding properties of materials for neutrons and photons: NGCal," *Radiat. Phys. Chem.*, vol. 185, Art. no. 109519, 2021.
[17] S. Islam, "MATXCOM—An X-ray/gamma-ray attenuation calculator for arbitrary materials based on EPICS2023 evaluated photon data library," *Radiat. Phys. Chem.*, vol. 229, Art. no. 112433, 2025.
[18] M. Aygun, Z. Aygun, and E. Ercan, "Radiation protection efficiency of newly produced W-based alloys: Experimental and computational study," *Radiat. Phys. Chem.*, vol. 212, Art. no. 111147, 2023.
[19] M. Kumar, N. P. Gurao, and A. Upadhyaya, "Implications of slip transition on the work hardening and texture evolution of nickel-tungsten-iron ternary alloy," *Mater. Charact.*, vol. 189, Art. no. 112010, 2022.
[20] T. Laas, K. Laas, J. Paju, J. Priimets, S. Tõkke, B. Väli, V. Shirokova, M. Antonov, V. A. Gribkov, E. V. Demina, V. N. Pimenov, M. Paduch, R. Matulka, and M. Akel, "Gamma behaviour of tungsten alloy with iron and nickel under repeated high temperature plasma pulses," *Fusion Eng. Des.*, vol. 151, Art. no. 111408, 2020.
[21] M. R. Kaçal, H. Polat, M. Oltulu, F. Akman, O. Agar, and H. O. Tekin, "Gamma shielding and compressive strength analyses of polyester composites reinforced with zinc: An experimental, theoretical, and simulation-based study," *Appl. Phys. A*, vol. 126, Art. no. 205, 2020.
[22] Q. Chang, S. Guo, and X. Zhang, "Radiation shielding polymer composites: Ray-interaction mechanism, structural design, manufacture and biomedical applications," *Mater. Des.*, vol. 233, Art. no. 112253, 2023.
[23] I. Celik, "Analysis of ionizing charged-particle shielding and range: Compilation for space exploration, medical physics, and nuclear safety," *Eur. Phys. J. Plus*, vol. 140, Art. no. 488, 2025.
[24] M. Joyce, "Fundamentals of Radioactivity," in *Nuclear Engineering: A Conceptual Introduction to Nuclear Power*. Oxford, U.K.: Butterworth-Heinemann, 2018, ch. 3, pp. 35–60.
[25] M. Abbas, A. El-Khatib, M. Elsafi, S. El-Shimy, M. Dib, H. Abdellatif, R. Baharoon, and M. Gouda, "Investigation of gamma-ray shielding properties of bismuth oxide nanoparticles with a bentonite–gypsum matrix," *Materials*, vol. 16, Art. no. 2056, 2023.

[26] G. Mahmoud, M. Sayyed, A. Almuqrin, J. Arayro, and Y. Maghrbi, "Monte Carlo investigation of gamma radiation shielding features for $Bi_2O_3$/epoxy composites," *Appl. Sci.*, vol. 13, Art. no. 1757, 2023.
[27] N. Ekinci, K. Mahmoud, B. Aygun, M. Hessien, and Y. Rammah, "Impacts of the colemanite on the enhancement of the radiation shielding capacity of polypropylene," *J. Mater. Sci.: Mater. Electron.*, vol. 33, pp. 20046–20055, 2022.
[28] R. Patel, G. Karthik, and P. Sharma, "Processing, microstructure, and mechanical behavior of tungsten heavy alloys for kinetic energy penetrators: A critical review," *J. Manuf. Mater. Process.*, vol. 9, no. 2, Art. no. 186, 2025.
[29] W. Zhu, W. Liu, Y. Ma, Q. Cai, J. Wang, and Y. Duan, "Low-temperature sintering of 90W–7Ni–3Fe alloy with Cu additive: Microstructure evolution and mechanical properties," *J. Mater. Res. Technol.*, vol. 11, pp. 2037–2048, 2021.
[30] J. Saemathong, N. Pannucharoenwong, V. Mongkol, S. Vongpradubchai, and P. Rattanadecho, "Analyzing two laser thermal energy calculation equations: A comparison of Beer–Lambert's law and light transport equation," *Eng. Sci.*, vol. 24, Art. no. 912, 2023.
[31] H. Jho, B. Lee, Y. Ji, and S. Ha, "Discussion for the enhanced understanding of the photoelectric effect," *Eur. J. Phys.*, vol. 44, Art. no. 025301, 2023.
[32] D. Salehi, D. Sardari, and M. Jozani, "Investigation of some radiation shielding parameters in soft tissue," *J. Radiat. Res. Appl. Sci.*, vol. 8, pp. 439–445, 2015.
[33] A. Souza, F. Aristone, A. Santana, A. Myai, F. Cion, P. Tsakiropoulos, and J. Rossi, "Characterization and determination of the gamma radiation attenuation coefficient in the W20Cu3Ni metallic alloy to be applied in the transport of radioactive substances," *J. Mater. Res. Technol.*, vol. 21, pp. 951–960, 2022.
[34] J. Lin, D. Cui, X. Li, C. Zou, J. Wu, C. Ren, and J. Chen, "Thermal neutron shielding properties of rare-earth nickel alloy materials," *Nucl. Mater. Energy*, vol. 44, Art. no. 101969, 2025.
[35] N. Salman and K. K. Hammud, "Phy-X/PSD and NGCAL models of several metal sulphides: Theoretical prediction of gamma shielding efficiency," *Iraqi J. Ind. Res.*, vol. 11, no. 3, pp. 94–118, 2024.